

# Tephra fallout hazard assessment at the Campi Flegrei caldera (Italy)

A. Costa · F. Dell’Erba · M. A. Di Vito · R. Isaia ·  
G. Macedonio · G. Orsi · T. Pfeiffer

Received: 9 April 2007 / Accepted: 9 May 2008 / Published online: 5 June 2008  
© Springer-Verlag 2008

**Abstract** Tephra fallout associated with renewal of volcanism at the Campi Flegrei caldera is a serious threat to the Neapolitan area. In order to assess the hazards related with tephra loading, we have considered three different eruption scenarios representative of past activity: a high-magnitude event similar to the 4.1 ka Agnano-Monte Spina eruption, a medium-magnitude event, similar to the ~3.8 ka Astroni 6 eruption, and a low-magnitude event similar to the Averno 2 eruption. The fallout deposits were reconstructed using the HAZMAP computational model, which is based on a semi-analytical solution of the two-dimensional advection–diffusion–sedimentation equation for volcanic tephra. The input parameters into the model, such as total erupted mass, eruption column height, and bulk grain-size and components distribution, were obtained by best-fitting field data. We carried out tens of thousands simulations using a statistical set of wind profiles, obtained from NOAA re-analysis. Probability maps, relative to the considered scenarios, were constructed for several tephra loads, such as 200, 300 and 400 kg/m<sup>2</sup>. These provide a hazard assessment for roof collapses due to tephra loading that can be used for risk mitigation plans in the area.

**Keywords** Tephra fallout hazard · Tephra loading · Campi Flegrei caldera

## Introduction

Around the world, many towns, cities and even megacities have been growing around and above active volcanoes. In these areas, volcanic hazards assessment needs to be carried out and it is imperative that zoning and development of the surrounding territory takes the risks into account. Volcanic eruptions can cause several hazardous phenomena, such as tephra fallout, pyroclastic density currents (PDC), lavas and lahars. The effects of such phenomena vary according to the size of the eruption and the distance from the eruption vent. In particular, tephra fallout load can generate structural damages to buildings where its value exceeds the threshold load. Even deposition of a thin tephra blanket can produce very dangerous effects to infrastructures, viability, agriculture, livestock and humans (Blong 1984; Tilling 1989). Moreover volcanic particles in the atmosphere may significantly affect air traffic (Casadevall 1994; Miller and Casadevall 2000) and may even induce changes in the climatic conditions (Mills 2000; Rampino and Self 2000; Fedele et al. 2003).

Forecasting type and size of the next eruption of a given volcano is a very arduous task in volcanic hazards assessment. Such forecasting cannot be performed deterministically, but only via a probabilistic approach. This can be based on simplified computational modelling of the variable possible scenarios.

The Neapolitan area, including the city of Naples, has a population of about four million people and has been growing over the past few millennia around, above and within three active volcanoes: Campi Flegrei, Somma-Vesuvius and Ischia (Orsi et al. 2003). Therefore, it is prone to severe volcanic hazards if there is renewal of volcanism at any of the three active volcanoes (Fig. 1). The fallout hazards associated with Somma-Vesuvius have been the

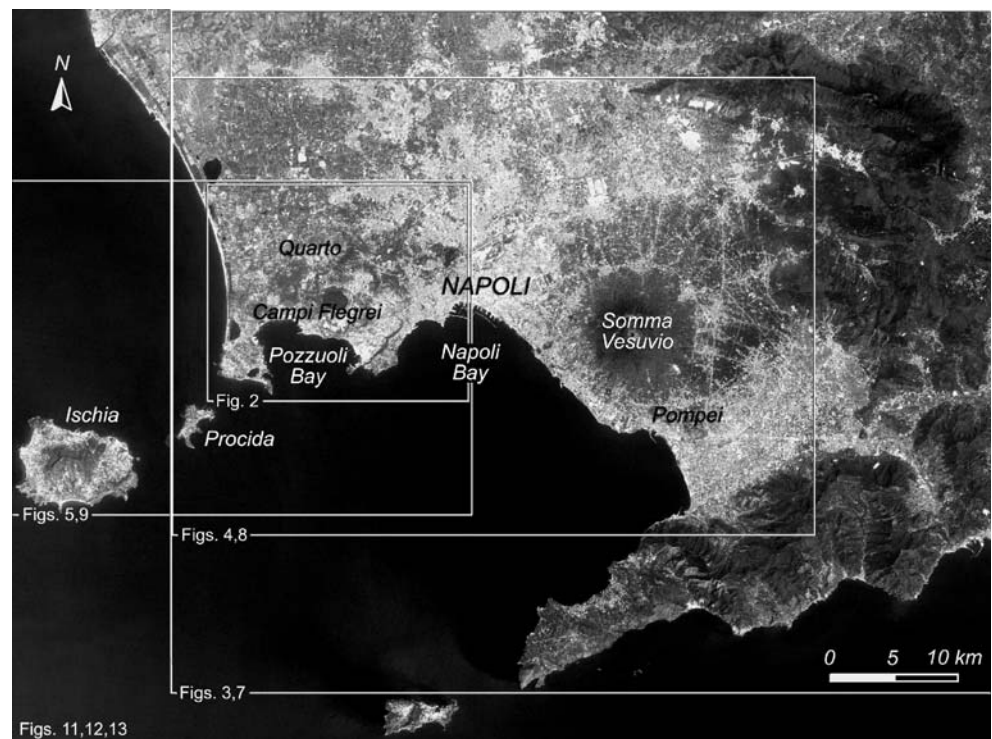
---

Editorial responsibility: R Cioni

---

A. Costa (✉) · F. Dell’Erba · M. A. Di Vito · R. Isaia ·  
G. Macedonio · G. Orsi · T. Pfeiffer  
Osservatorio Vesuviano, Napoli,  
Istituto Nazionale di Geofisica e Vulcanologia,  
Via Diocleziano 328,  
80124 Naples, Italy  
e-mail: costa@ov.ingv.it

**Fig. 1** The Neapolitan area with reference frames for Figs. 2, 3, 4, 5, 7, 8, 9 and 11, 12, 13. 23 July 2004 Landsat 7 image (Sensor ETM+) from ESA, processed by laboratory of Geomatics and Cartography of INGV-OV



subject of several papers (e.g., Barberi et al. 1990; Macedonio et al. 1990; Lirer et al. 2001; Cioni et al. 2003). However, only very few attempts have been made to assess the hazards posed by a future volcanic activity from the Campi Flegrei caldera (e.g., Orsi et al. 2004 and references therein).

This paper is based on the volcanic hazards assessment in case of renewal of volcanism at the Campi Flegrei caldera (CFc) in short-mid terms proposed by Orsi et al. (2004), and is focussed on assessing the fallout hazard for the Neapolitan area. As previously mentioned, tephra transport and fallout can generate a large spectrum of hazards. A complete evaluation of such hazards at the CFc is out of the scope of this paper. Our focus is mainly the probabilistic assessment of tephra fallout loadings exceeding the thresholds that can cause serious damage to buildings in that area.

The reference eruptions for three different sizes of events have been selected following Orsi et al. (2007). Here, our major task is twofold. One goal is to apply the semi-analytical model HAZMAP (Macedonio et al. 2005; Pfeiffer et al. 2005) to the reference eruptions for the high, medium- and low-magnitude scenarios expected at CFc, in order to simulate tephra dispersion and deposition from sustained eruption columns. The second objective is to construct tephra load probability maps on the basis of best fit parameters defining the three eruptions, and a statistical dataset of wind profiles. The wind dataset contains the daily-average wind profiles corresponding to the point of the NCEP/NCAR (Kalnay et al. 1996) global mesh nearest

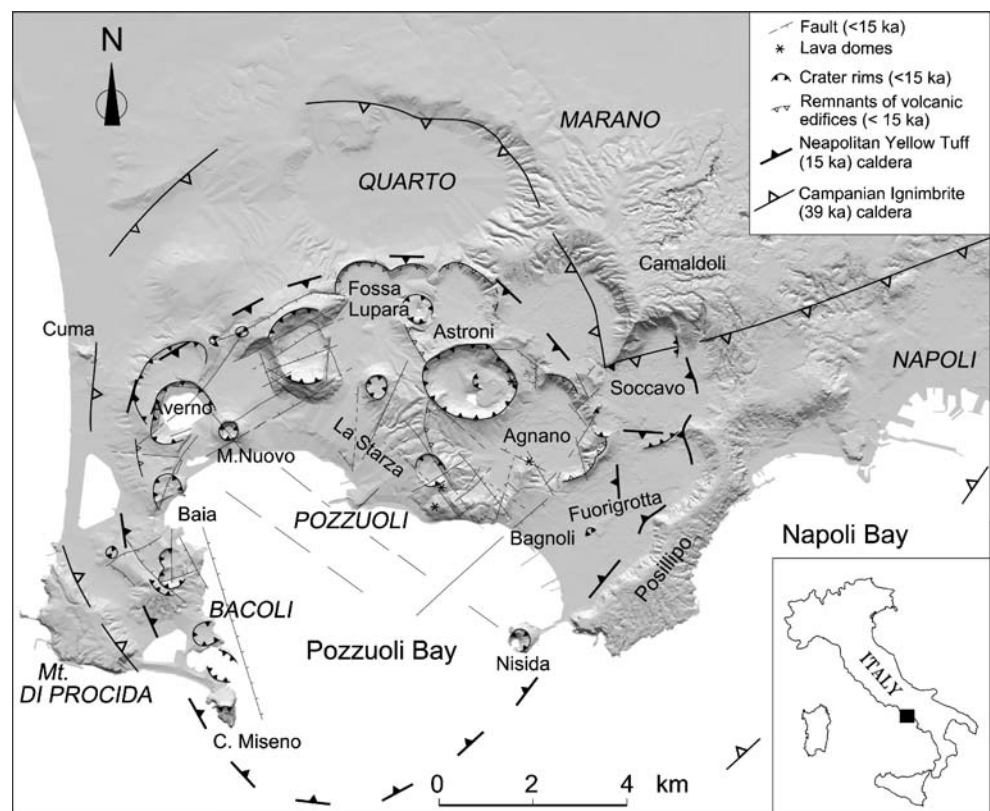
to Naples (latitude=40° N, longitude=15° E) as given by the NCEP/NCAR re-analysis (<http://www.cdc.noaa.gov/cdc/reanalysis/>) for the period 1968 to 2003 (36 years).

In the first part of this paper we describe the evolution and the present state of the CFc, and in particular the three reference eruptions chosen on the basis of the past activity. Then we discuss the results obtained applying the semi-analytical model HAZMAP to simulate and analyse the deposits of the three eruptions. Finally, we present probability tephra-fallout distribution and loading maps.

### The CFc: evolution, present state and volcanic hazards

The CFc is a nested structure which formed during two main collapses associated with the Campanian Ignimbrite (39 ka; Fisher et al. 1993; Civetta et al. 1997; Rosi et al. 1996; De Vivo et al. 2001; Ort et al. 2003) and Neapolitan Yellow Tuff (15 ka; Orsi et al. 1992; 1995; Wohletz et al. 1995; Deino et al. 2004) eruptions (Fig. 2; Orsi et al. 1996). Volcanism in the last 15 ka occurred within the younger caldera, and was concentrated in three epochs (15–9.5, 8.6–8.2, 4.8–3.8 ka) separated by two periods of quiescence (Di Vito et al. 1999). The last event occurred in AD 1538, with the formation of Monte Nuovo. This volcanism has generated about 70 eruptions, which were mainly explosive with only four recognized effusive events. The whole structure is presently subsiding, while the central part of the Neapolitan Yellow Tuff caldera is affected by resurgence, with a net vertical uplift of 90 m (Orsi et al. 1996).

**Fig. 2** Map of the main volcanic and volcano-tectonic features of the CFc. After Di Vito et al. (1999)



The distribution of the eruption vents through time is strictly related to the dynamics of the caldera deformation (Orsi et al. 1996, 1999). The Neapolitan Yellow Tuff caldera has been affected by ground deformation over the past 2 ka (Orsi et al. 1999 and references therein). Two major unrest episodes occurred between 1969 and 1972, and 1982 and 1984, which generated 170 and 180 cm of maximum ground deformation, respectively. They were followed by smaller episodes of inflation in 1989 (7 cm), 1994 (<1 cm), 2000 (4 cm), and 2006 (4 cm).

The CFc is currently in a persistent state of activity, as testified by the last eruption of Monte Nuovo, the recent unrest episodes, and the intense fumarolic activity (Orsi et al. 2004 and references therein). This current state of activity and the explosive character of the system make the potential for volcanic hazards very high. The presence of a large population in the surrounding Neapolitan area makes the volcanic risk among the highest in the world.

Explosive eruptions of the past 15 ka have been grouped into three size classes: low-, medium- and high-magnitude events (Orsi et al. 2004, 2007). Violent Strombolian, sub-Plinian and Plinian type eruptions correspond to the defined low-, medium-, and high-magnitude size classes. The explosive eruptions were predominantly phreatomagmatic, or alternated between magmatic and phreatomagmatic phases. Expanded and turbulent PDCs and tephra fallout were generated during phreatomagmatic and magmatic explosions. Areal distribution of the resulting pyroclastic

deposits was dictated by variable factors (Orsi et al. 2004, 2007). The PDC deposits were laid down within the caldera floor or outside the caldera rim, according to both magnitude and vent location of the eruption. The fallout deposits of the low- to medium-magnitude eruptions were dispersed in many directions but mainly towards the northeast, while those of Plinian columns were dispersed towards the east.

Most of the explosive eruptions were low- or medium-magnitude events and dispersed their products over areas ranging from a few to 500 km<sup>2</sup>, while the highest magnitude Plinian events, namely Pomici Principali (10.3 ka; Lirer et al. 1987; Di Vito et al. 1999) and Agnano-Monte Spina (AMS; 4.1 ka; De Vita et al. 1999), dispersed their products over areas >1,000 km<sup>2</sup> (Orsi et al. 2004; Orsi et al. 2007).

The reconstructed behaviour of the CFc, including its magmatic feeding system, the magnitude of the explosive eruptions of the past 15 ka and their variation through time, allowed Orsi et al. (2004) and Orsi et al. (2007) to conclude that the most probable future event would be similar to the previous low- or medium-magnitude events. The largest expected eruption is taken to be similar to the AMS event. In particular, probabilities of ~15% for a purely effusive eruption, ~50% for a low-magnitude event, ~30% for a medium-magnitude event, and ~5% for a high-magnitude event were estimated by Selva et al. (2007).



Orsi et al. (2004) suggested that the direct hazards expected from an explosive eruption include tephra fallout and dilute and turbulent PDC. They constructed a PDC and a tephra-fallout hazard map, in addition to a vent opening hazard map. The PDC hazard map was constructed using the areal distribution and frequency of the past PDC deposits. While the tephra fallout hazard map was based on frequency of both deposition of fallout beds and frequency of tephra load on the ground, direction of dispersal axis, and limit load of collapse for the variable roof typologies in the area (about 200, 300, 400 and 500 kg/m<sup>2</sup>).

### The reference eruptions for fallout hazard assessment

In order to perform the tephra-fallout hazard assessment related to renewal of volcanism at the CFC in short-mid terms, we selected the AMS, the Astroni, and the Averno 2 eruptions as representative of the high-, medium- and low-magnitude eruption scenarios, following Orsi et al. (2004) and Orsi et al. (2007). In particular we have studied the main fallout deposits (B1 and D1) of AMS (De Vita et al. 1999), Unit 6 of the Astroni sequence (Isaia et al. 2004), and the A2 fallout layer of the Averno 2 eruption (Di Vito et al. 2004). It is worth noting that, for each scenario, the three reference eruptions, have the largest amounts of fallout deposits, among those detected in the field for the last 5 ka (Orsi et al. 2004). Since even for the low-magnitude Averno 2 eruption there are compelling field evidence that a sustained column developed, the application of the semi-analytical HAZMAP model can be considered appropriate.

**Agnano Monte Spina eruption** The AMS is the highest-magnitude eruption that occurred over the past 5 ka within the CFC (Rosi et al. 1983; Di Girolamo et al. 1984; Rosi and Santacroce 1984; Rosi and Sbrana 1987; De Vita et al. 1999; Di Vito et al. 1999; Dellino et al. 2001; Orsi et al. 2004, 2007). De Vita et al. (1999) presented a detailed reconstruction of the pyroclastic sequence and constrained the age of the eruption to 4.1 ka. Variation of lithological features allowed the authors to subdivide the whole sequence into six members (A through F). Members are further subdivided into sub-members upon sedimentological characteristics. Plinian/sub-Plinian fallout deposits generated by magmatic explosions frequently alternate with base-surge beds of phreatomagmatic origin (De Vita et al. 1999; Dellino et al. 2004). During some eruption phases the contrasting eruption dynamics were almost contemporaneous (Dellino et al. 2004). On the basis of the stratigraphic sequence, the history of the eruption was also reconstructed (De Vita et al. 1999).

Only two of the six members of the AMS pyroclastic sequence comprise coarse fallout layers produced during Plinian phases. The stratigraphically lowest Plinian fallout deposit of the entire AMS sequence was recognized at the base of Member B (sub-Member B1). It is composed of a coarse pumice-fallout layer laid down by a pulsating column reaching a maximum height of about 23 km. Isopach maps indicate that B1 was dispersed towards the east up to 45 km from the vent area (Fig. 3). Another coarse pumice-fallout deposit (sub-Member D1) was recognized in the lower portion of the Member D. This fallout layer generated during magmatic explosions was deposited by a Plinian column that reached a maximum height of about 30 km. Layer D1 is a pumice-fallout deposit with a northeastward oriented dispersal axis. Isopachs are quite regular elliptical curves covering an area of at least 700 km<sup>2</sup> (Fig. 3). According to De Vita et al. (1999), thickness of AMS Tephra varies from a maximum estimated value of about 70 m in the Agnano plain, which is the inferred vent area, to a few centimetres over a distance of about 50 km (Fig. 3). The total volume of the erupted magma was 1.2 km<sup>3</sup> (DRE), while a volume of 0.11 and 0.10 km<sup>3</sup> (DRE) was here estimated for B1 and D1 fallout deposits, respectively.

**Astroni eruptions** The Astroni volcano, a well preserved elliptical edifice on the north-western margin of the AMS collapse area (Fig. 2), formed during 7 eruptions of variable magnitude, two of which ended with low-energy explosions and lava extrusions (Isaia et al. 2004). Radiometric, stratigraphic, and archaeological data constrain the age of the construction of Astroni volcano between 4.1 and 3.8 ka

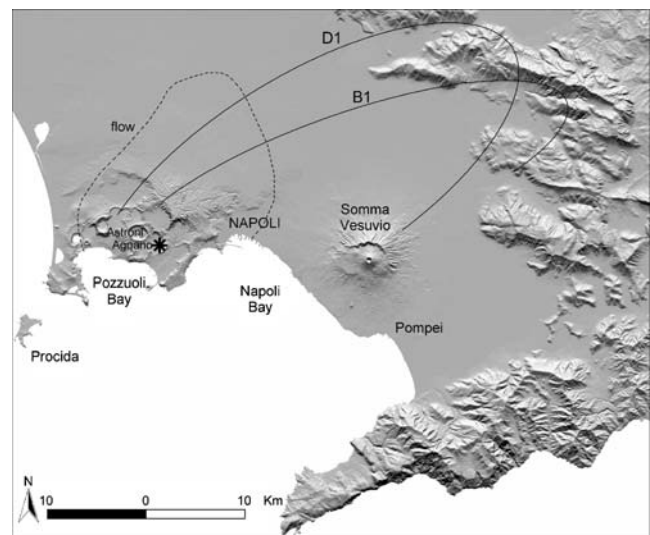


**Fig. 3** Areal distribution of Agnano Monte Spina deposits; the dashed line delimits the area of the PDC dispersion, the solid lines encompass the isopachs of 10 cm for the main fallout deposits, the asterisk indicates the vent area. After De Vita et al. (1999)

BP. This implies that the 7 eruptions closely followed each other in time. The estimated volume of the whole Astroni sequence is  $1.02 \text{ km}^3$ , which corresponds to  $0.45 \text{ km}^3$  of erupted magma (DRE). The volume of erupted magma for each of the Astroni eruptions varies between  $0.13$  and  $0.01 \text{ km}^3$  (DRE). These variable magnitude Astroni eruptions are taken to represent the medium- and low-magnitude events defined by Orsi et al. (2004).

The 7 eruptions were predominantly phreatomagmatic with subordinate magmatic phases. They generated 7 units (named 1 through 7, from base upwards) that are separated by either thin paleosols or erosional unconformities. The units are composed of ash to coarse-ash surge beds and subordinate fallout layers. Only two units (5 and 7) include Strombolian scoria deposits and lavas. The surge beds were deposited by dilute and turbulent PDCs, generally confined to the CFc depression, whereas fallout layers were laid down from low eruption columns and dispersed also outside the caldera, towards the north and east (Fig. 4). All the phreatomagmatic explosions generated large amount of ash. The texture of their deposits varies with distance from the vent, from coarse and wavy to plane-parallel, to fine and plane-parallel, and then finally to massive farthest from vent.

Astroni Unit 6 (A-U6) is mostly composed of fine- to coarse-ash surge beds, with minor fallout layers. It includes a coarse basal pumice-fallout deposit generated during a magmatic phase of the eruption. This deposit made up by alternated coarse pumice layers and fine-ash beds, was dispersed towards the east, up to a distance of about 20 km from the vent (Fig. 4). Following the model of Carey and

Sparks (1986), a maximum column height of about 14 km was estimated. The volume of A-U6 was estimated around  $0.1 \text{ km}^3$  (DRE), while the volume of the basal pumice fallout is about one fifth of total volume (Isaia et al. 2004).

**Averno eruption** The Averno 2 (Av2) Tephra (3.8 ka) is one of the best exposed pyroclastic sequence in the western sector of the CFc (Rosi and Sbrana 1987; Di Vito et al. 1999, 2004; Orsi et al. 2004). The eruption was characterised by magmatic and phreatomagmatic explosions which produced a sequence of pyroclastic-fall and surge deposits. Following Di Vito et al. (2004), the whole sequence includes three members named A through C. Member A was emplaced during the first phase of the eruption by prevailing magmatic explosions which generated six fallout beds. The subsequent phases of the eruption generated explosions driven by variably efficient water–magma interaction with formation of wet to dry surges, which emplaced Member B and C (Fig. 5). Isopachs and isopleths maps of fallout deposits, as well as areal distribution of both ballistic fragments and surge beds facies, suggest a vent migration during the eruption from southwest to northeast, likely along a NE–SW fault system.

Fallout deposits of Member A were laid down by eruption columns which reached maximum heights between 8 and 10 km, calculated using the Carey and Sparks (1986) method. However, areal distribution is poorly constrained due to both dispersal of the plume mostly over the sea, and paucity of measurable outcrops on land. The basal layer A0 is a coarse-grained, poorly-sorted fallout deposit (A0f) overlain by a sequence of massive, cohesive, coarse- to fine-ash surge beds (A0s). Layer A1 includes a well-sorted fallout deposit (A1f), containing angular pumice lapilli, and a yellowish fine- to coarse-ash bed (A1s). Layer A2

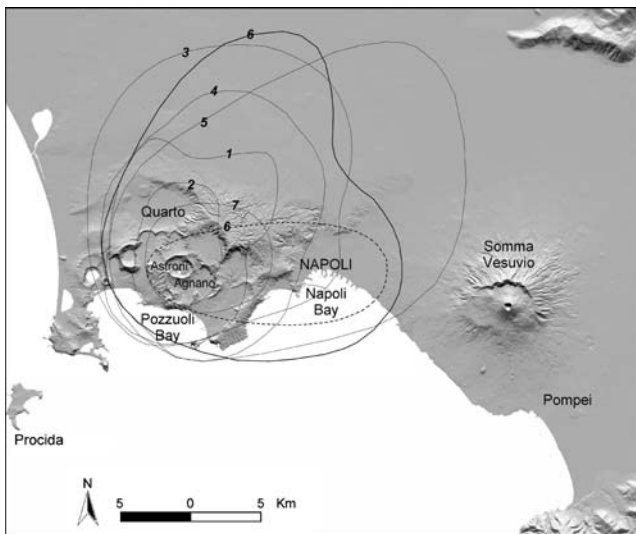


**Fig. 4** Areal distribution of the deposits of the 7 units of Astroni volcano (solid lines). The thicker line includes the distribution of the whole Astroni 6 Unit. The dashed line encompasses the 10 cm isopach of the coarse fallout deposit of Unit 6 (A-U6). After Isaia et al. (2004)

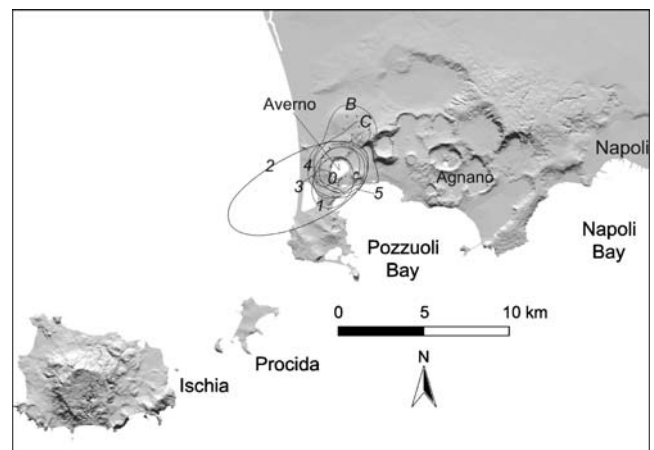


**Fig. 5** Areal distribution of the deposits of the Av2 eruption. Curve labels 0 to 5 denote the 10 cm isopachs of the fallout deposits of Member A. Curve labels B and C indicate the distributions of whole B and C members. The thicker line (label 2) encompass the fallout deposit A2f

includes a well sorted, reverse- to normal-graded coarse pumice fallout deposit (A2f) overlain by surge beds (A2s). The isopachs of A2f fallout, that is the widest distributed deposit of the Av2 Tephra, show a dispersal toward southwest. Layers A3, A4 and A5 are composed of well-sorted coarse pumice fallout deposits capped by fine- to coarse-ash beds.

Members B and C are dominated by sequences of surge beds with subordinate fallout layers. In particular Member B is composed of cohesive, massive to cross-laminated, generally fine-ash beds, containing abundant accretionary lapilli, laid down mainly by wet-surge currents. The currents flowed preferentially towards the north over an area of about 34 km<sup>2</sup>. Member C is composed of a sequence of cross-laminated, coarse- to fine-ash beds and poorly sorted lapilli-sized pumice fallout deposits, and minor thin, gray to purple, accretionary lapilli rich, fine-ash beds. Member C was mainly dispersed towards the north over an area of about 12 km<sup>2</sup>, by dry-surge currents and subordinate short-lived eruption columns.

The dispersal area of the fallout deposits of Member A varies between 14.7 (A3f) and 36.8 km<sup>2</sup> (A2f). The estimated volumes of A1f and A2f are 0.001 and 0.008 km<sup>3</sup> (DRE), respectively, while those of Members A, B and C are 0.016, 0.023, and 0.027 km<sup>3</sup> (DRE).

### Tephra deposition modelling and governing parameters

Dispersion and sedimentation of particles from a sustained eruption column in distal areas, can be fairly well determined from wind transport, turbulent diffusion, and settling by gravity. Assuming a constant and horizontally uniform wind field, and a negligible vertical diffusion coefficient, the mass conservation equation for each class of particles with a given settling velocity  $V_{sj}$  can be written as:

$$\frac{\partial C}{\partial t} + W_x \frac{\partial C}{\partial x} + W_y \frac{\partial C}{\partial y} - \frac{\partial (V_{sj} C)}{\partial z} = K \left( \frac{\partial^2 C}{\partial x^2} + \frac{\partial^2 C}{\partial y^2} \right) + S_j \quad (1)$$

where  $C$  is the particle concentration,  $(W_x, W_y)$  the wind field,  $K$  the horizontal turbulent diffusion coefficient (assumed constant), and  $S_j$  the source term related to the eruption column. A purely empirical description that reproduces the geometrical shape of an eruption column was adopted (Macedonio et al. 2005; Pfeiffer et al. 2005). In this model, the eruption column acts as a vertical line source. Since this simplification is only valid in distal area, the use of the model is limited accordingly. In particular, previously obtained results (Macedonio et al. 1988; Armienti et al. 1988) suggest that the critical distance is

approximated by the height of the eruption column itself. Equation 1 was solved by using a semi-analytical solution as described in Macedonio et al. (2005) and Pfeiffer et al. (2005).

Governing parameters in Eq. 1 were obtained by best fit with field data as described in Pfeiffer and Costa (2004a, b) for AMS, A-U6 deposits. The same approach was adopted for the case of the Av2 eruption using field data by Di Vito et al. (2004). The best fit with the studied deposits allows us to estimate: total mass associated with tephra fallout, eruption column height, bulk particle settling velocity distribution, column shape parameters, diffusion coefficients and wind velocity.

The model parameters, were defined by minimising the Standard Deviation of Regression:

$$\sigma^2 = \frac{1}{N - p} \sum_{i=1}^N w_i [Y_{\text{obs},i} - Y_{\text{mod},i}]^2 \quad (2)$$

where  $w_i$  are weighting factors,  $N$  is the number of data points,  $p$  is the number of free parameters,  $Y_{\text{obs},i}$  denote the observation data (e.g., detected deposit thicknesses) and  $Y_{\text{mod},i}$  the values predicted by the model. The choice of the weighting factors  $w_i$  depend upon the distribution of the errors. If all the measurements have equal uncertainty uniform weighting factors ( $w_i=1$ ) has to be used. If, however, the measurements have different uncertainties, proportional weighting factors ( $w_i = 1/Y_{\text{obs},i}^2$ ) or statistical weighting factors ( $w_i = 1/Y_{\text{obs},i}$ ) should be used (e.g. Aitken 1935). The statistical weight  $w_i = 1/Y_{\text{obs},i}$  is a compromise between a uniform and a proportional weight, and it is appropriate when  $Y_{\text{obs},i}$  follow a Poisson distribution. Generally, the best weighting factor is the one that yields a random residual plot with no functional dependencies. For simplicity, we have adopted a proportional weighting factor, following Pfeiffer et al. (2005).

The results of the best fit procedure for the AMS and A-U6 Phlegrean eruptions considered, are reported in Pfeiffer and Costa (2004a) and Pfeiffer and Costa (2004b), respectively. Tephra thickness values and grain size distributions of Av2 eruption from Di Vito et al. (2004) were used for the numerical reconstruction of the main fallout deposit. A plot of the observed tephra deposit thickness against the calculated deposit thickness is reported in Fig. 6 for all three the eruptions. The final set of input parameters used for the model for each scenario is reported in Table 1.

The input parameters chosen for the AMS eruption were obtained from a weighted average of the best parameters for B1 and D1 levels obtained in Pfeiffer and Costa (2004a). The total mass was cautiously chosen to equal the sum of mass associated with both B1 and D1 fallout, i.e.  $5.2 \times 10^{11}$  kg (0.2 km<sup>3</sup> DRE).

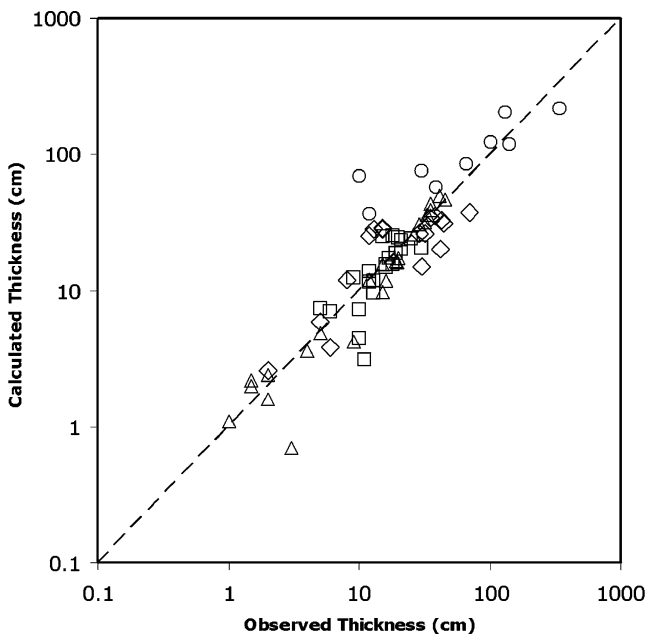


**Fig. 6** Log–Log plot of the observed tephra deposit thickness against the calculated deposit thickness for the three eruptions studied. *Open triangles* and *open squares* represent AMS-B1 and AMS-D1 deposits, respectively. *Open diamond* refer to data of A-U6 deposits, whereas *open circles* indicate Av2-A2f deposits

Concerning the Astroni eruption scenario, a bulk mass of about  $4.1 \times 10^{10}$  kg ( $0.016 \text{ km}^3$  DRE) for the basal coarse layer of A-U6 fallout deposit was calculated by Pfeiffer and Costa (2004b) through a best fit with field data.

The mid-distal deposits of many Phlegraean explosive eruptions are composed of massive fine ash, likely laid down by both sustained columns and continuous suspensions in the upper part of PDCs. These two components usually cannot be accounted for separately. We concur with Orsi et al. (2004) including the structureless ash beds that could have been deposited by the upper part of the PDCs because their effects on the territory, lacking horizontal component of the transport, can be assumed as similar to that of the falling tephra. As far as modelling concerns this criterion implies an overestimation of the mass in the sustained column. Although this should affect the description of the column and it should be treated with a more elaborated PDC model which is a topic out of the scope of this paper, it gives a more realistic estimate of the ash-load on the ground. For these reasons, in the Astroni eruption scenario, the mass of the total fine ash outside the CFC, comprising both the mid-upper beds of the fallout deposit and the ash beds produced during the final phase of the eruption, was cautiously added. On the basis of the thickness, volume and density of the deposits (Isaia et al.

**Table 1** Input parameters used for probability maps construction

Model parameters	Scenario type		
	High-magnitude (Plinian) “AMS (B1+D1)”	Medium-magnitude (sub-Plinian) “ASTRONI (U6)”	Low-magnitude (violent Strombolian) “AF2”
Total mass	$5.2 \times 10^{11}$ kg	$1.2 \times 10^{11}$ kg <sup>a</sup>	$2.3 \times 10^{10}$ kg
Column height	26 km	12 km	7 km
Column shape coefficients: $A/\lambda$	4/1	4/1	3/1
Number of $V_{\text{sett}}$ -classes	6	6	6
Bulk settling velocity distribution: $V_{\text{sett}}$ (Wt%)	0.5 m/s (18); 2.5 m/s (52); 4.5 m/s (18); 6.5 m/s (6); 8.5 m/s (3); 10.5 m/s (3)	0.5 m/s (12); 2.5 m/s (28); 4.5 m/s (36); 6.5 m/s (17); 8.5 m/s (5); 10.5 m/s (2)	0.5 m/s (10); 2.5 m/s (16); 4.5 m/s (29); 6.5 m/s (26); 8.5 m/s (12); 10.5 m/s (7)
Diffusion coefficient $K$	5000 m <sup>2</sup> /s	5000 m <sup>2</sup> /s	1000 m <sup>2</sup> /s
Mass eruption rate	$\leq 10^8$ kg/s	$\leq 10^7$ kg/s	$\leq 10^6$ kg/s
Daily wind profiles (period 1968–2003)	NOAA (lat 40°; long 15°)	NOAA (lat 40°; long 15°)	NOAA (lat 40°; long 15°)
References	Pfeiffer and Costa (2004a)	Pfeiffer and Costa (2004b)	Di Vito et al. (2004)
Total mass using Pyle (1989)	$3.6 \times 10^{11}$ kg (B1) $5.1 \times 10^{11}$ kg (D1)	$1.0 \times 10^{11}$ kg <sup>a</sup>	$3.9 \times 10^{10}$ kg
Max column height using Carey and Sparks (1986)	23 km (B1); 27 km (D1)	14 km	10 km

Mass eruption rates, given by buoyant plume theory, total mass, calculated using Pyle (1989), and column height, estimated according to Carey and Sparks (1986), are also reported for completeness.

<sup>a</sup>Including fine ashes (see text for details)



2004; Orsi et al. 2004) this mass was estimated to be around  $8 \times 10^{10}$  kg. Hence, a total mass of  $1.2 \times 10^{11}$  kg, i.e.  $0.016 \text{ km}^3$  DRE (Table 1), was used for assessing the tephra load impact.

Finally, for what concerns the fallout phase of the Av2 eruption, we calculated a best fit mass of  $2.3 \times 10^{10}$  kg and a column height of about 7 km (Table 1).

The numerically reconstructed isopachs, for the eruptions considered above, are shown in the Figs. 7a, b, 8 and 9. Granulometric and component analyses, and further details are reported in Pfeiffer and Costa (2004a, b) and Di Vito et al. (2004).

Column height and total erupted mass obtained by best fit between model results and field data are similar to estimations provided by independent methods (Carey and Sparks 1986; Pyle 1989). On the base of the column height

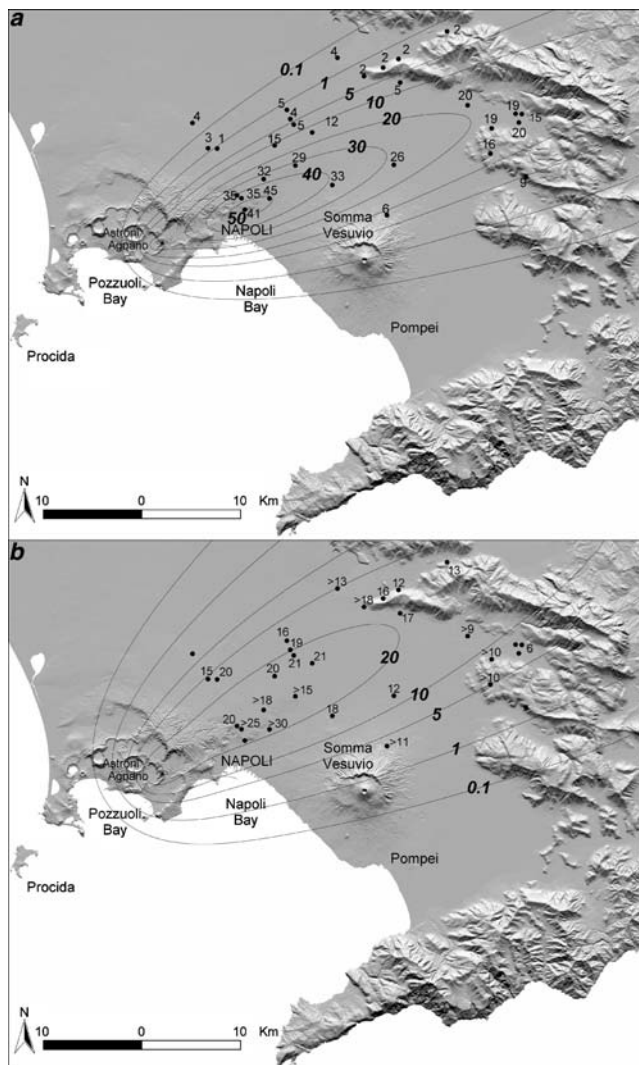


**Fig. 7** Calculated isopachs and measured thickness (cm) of **a** AMS-B1 and **b** AMS-D1 fallout deposits. After Pfeiffer and Costa (2004a)

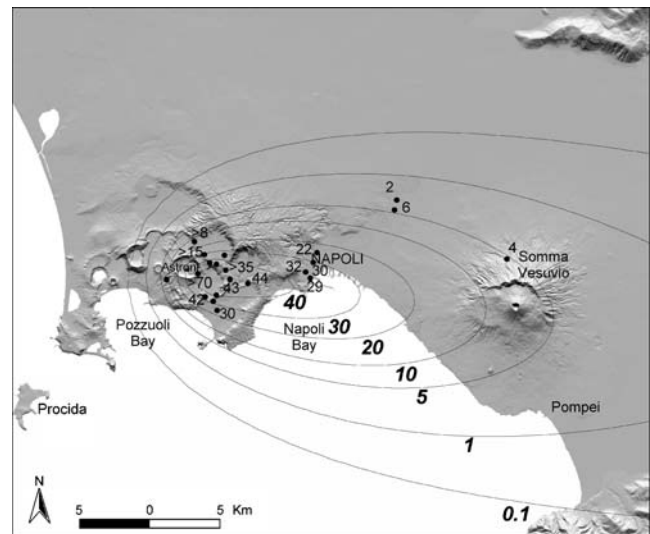


**Fig. 8** Calculated isopachs and measured thickness (cm) of A-U6 fallout deposits. After Pfeiffer and Costa (2004b)

characterizing each scenario, buoyant plume theory for volcanic columns (e.g., Sparks 1986; Bursik 2001) allowed us to estimate the mass flow rates reported in Table 1.

#### Computational approach for construction of probability maps

In order to construct tephra load probability maps, for the high-, medium- and low- magnitude eruption scenarios, we used the best fit parameters (described above) summarized in Table 1, and a statistical set of wind profiles representative of the Naples area (Fig. 10). The parameters used include: total mass, eruption column height, bulk particle settling velocity

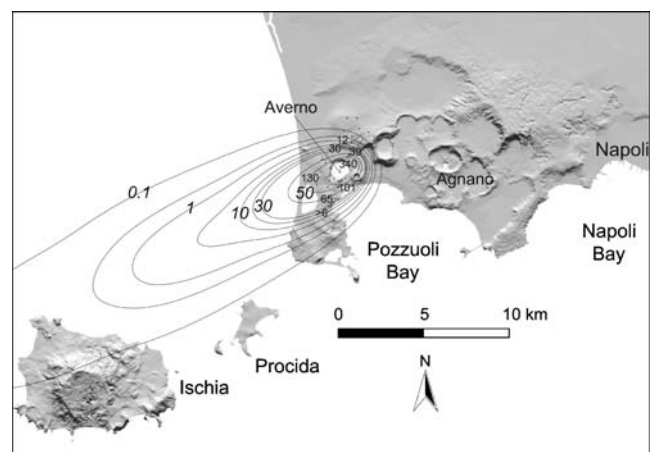


**Fig. 9** Calculated isopachs and measured deposit thickness (cm) of Av2-A2f fallout deposits



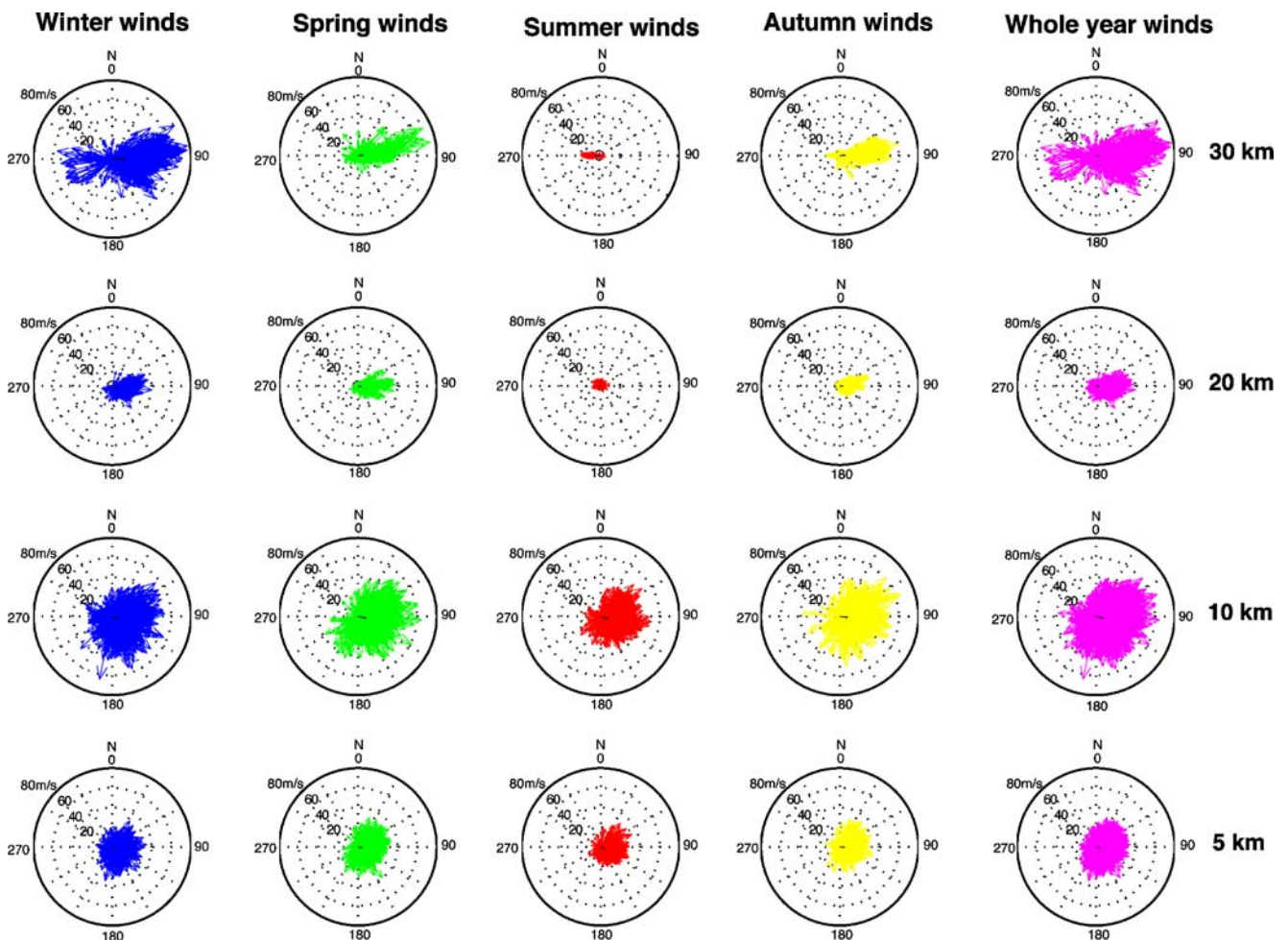


**Fig. 10** Wind distribution diagrams corresponding to the point of the NOAA global mesh nearest to Naples (140°, 15°) for the period 1968–2003 (36 years). Horizontal wind vectors (intensity and direction) are reported at the different altitudes (30 km, 20 km, 10 km and 5 km respectively). *Blue* corresponds to winter (January, February, March)

winds, *green* to spring (April, May, June) winds, *red* to summer (July, August, September) winds, *yellow* to autumn (October, November, December). *Magenta* corresponds to whole year winds that were used to obtain the probability maps. *Black arrows* denote the average values

distribution, column shape, and diffusion coefficients. Daily-average wind profiles were obtained from the NOAA global mesh nearest to Naples (40°N,15°E) as given by the NCEP/NCAR re-analysis (Kalnay et al. 1996) for the period 1968–2003 (<http://www.cdc.noaa.gov/cdc/re-analysis/>).

The statistical distribution of wind intensities and directions for the considered period at different representative heights are reported in Fig. 10. This figure also shows that for high eruption columns (around 30 km) prevailing winds blow mainly from West (about 80% of the barycentres of deposits would be comprised in a sector between NNE and SSE, whereas 10% only would be comprised in a sector between SSW and NNW). However, there is an evident wind seasonal variation consisting in both strong reduction in intensity and inversion in direction (wind blowing from east instead of west) during the Summer period. Below 10 km, wind distribution tends

to become less anisotropic although winds blowing from west remain the majority. Assuming that column shape parameters are not affected by wind profiles (that is valid for sustained eruptive column), we performed more than 13,000 simulations of the tephra deposits and we calculated the corresponding probability maps. Predicting the vent location for the next eruption at CFC is a very difficult task and only a probabilistic study is possible (Selva et al. 2007). Here, for sake of simplicity, only two locations for the eruption vent were accounted for. They were set in the centres of the Agnano-San Vito and Astroni-Monte Nuovo areas which were considered by Orsi et al. (2004) as the areas at higher and lower probability of vent opening at CFC. A comprehensive probabilistic analysis of vent locations on tephra fallout maps is the object of ongoing researches (e.g., Selva et al. 2007).

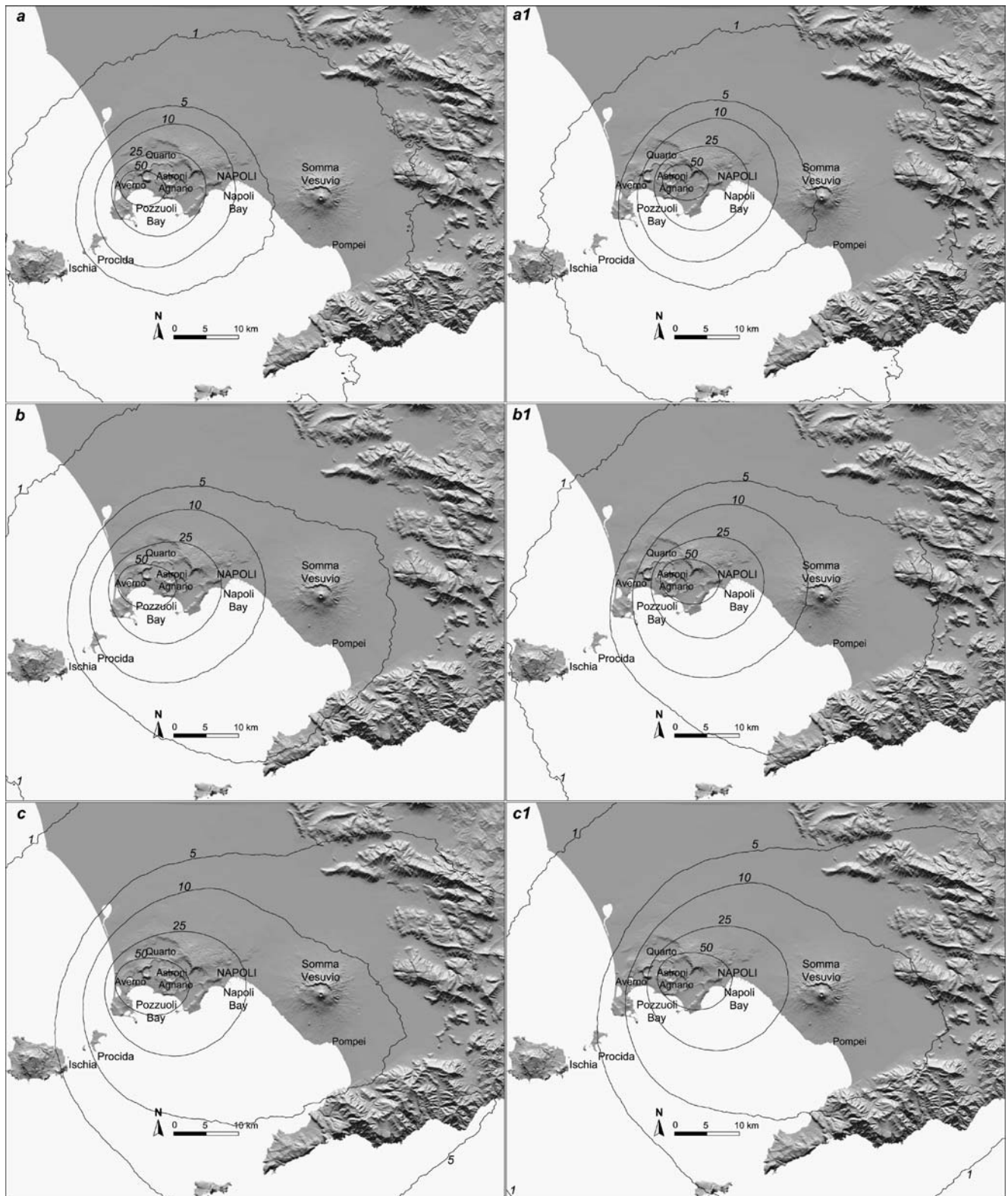


**Fig. 11** Ash loading probability maps for the high-magnitude scenario with an eruption vent in the Averno-Monte Nuovo area **a**  $400 \text{ kg/m}^2$ , **b**  $300 \text{ kg/m}^2$ , **c**  $200 \text{ kg/m}^2$ , and in the Agnano-San Vito area **a1**  $400 \text{ kg/m}^2$ , **b1**  $300 \text{ kg/m}^2$ , **c1**  $200 \text{ kg/m}^2$



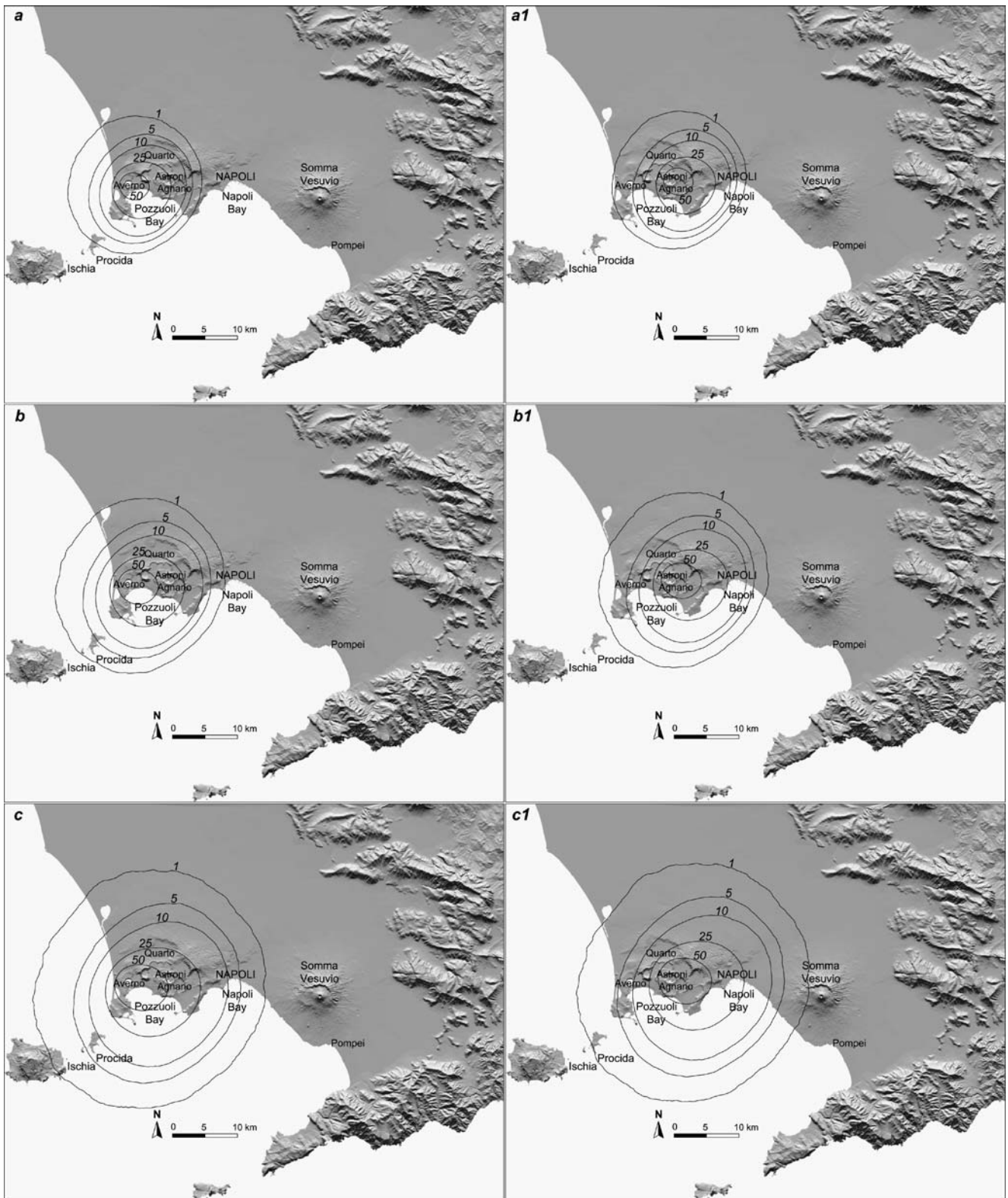


**Fig. 12** Ash loading probability maps for the medium-magnitude scenario with an eruption vent in the Averno-Monte Nuovo area **a** 400 kg/m<sup>2</sup>, **b** 300 kg/m<sup>2</sup>, **c** 200 kg/m<sup>2</sup>, and in the Agnano-San Vito area **a1** 400 kg/m<sup>2</sup>, **b1** 300 kg/m<sup>2</sup>, **c1** 200 kg/m<sup>2</sup>

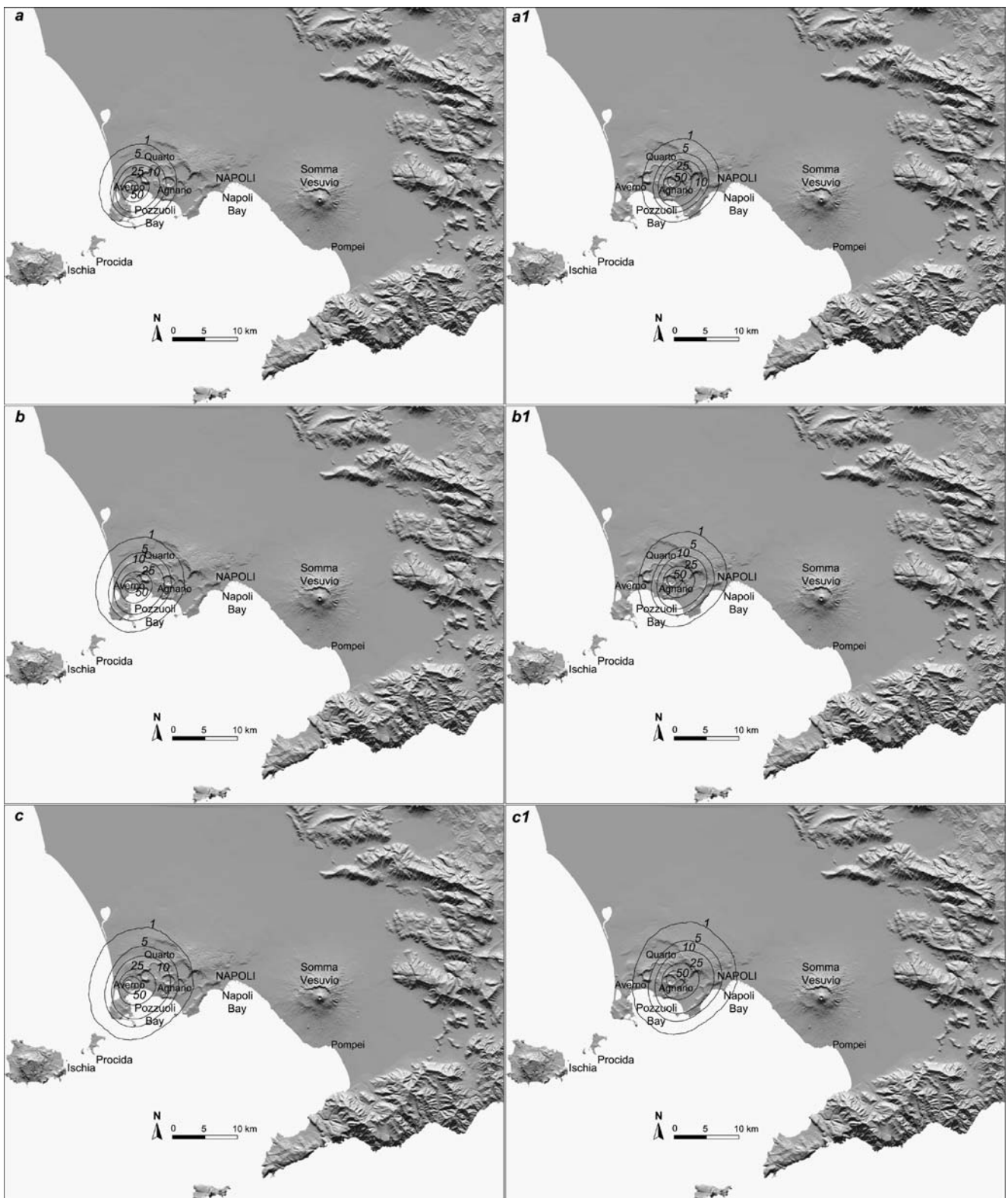


**Fig. 13** Ash loading probability maps for the low-magnitude scenario with an eruption vent in the Averno-Monte Nuovo area **a** 400 kg/m<sup>2</sup>, **b** 300 kg/m<sup>2</sup>, **c** 200 kg/m<sup>2</sup>, and in the Agnano-San Vito area **a1** 400 kg/m<sup>2</sup>, **b1** 300 kg/m<sup>2</sup>, **c1** 200 kg/m<sup>2</sup>



## Results and discussion

Using the procedure described above and the input parameters reported in Table 1 for the high-, medium- and low-magnitude scenarios, and a statistical set of re-analysis wind profiles (more than 13,000), we have constructed tephra loading probability maps for several thresholds from 100 to 1500 kg/m<sup>2</sup>. Here maps of loading thresholds of 400, 300, and 200 kg/m<sup>2</sup> (Figs. 11, 12 and 13) are presented and discussed. These thresholds values are the critical loads for roof collapse for different buildings in the Neapolitan area (Pareschi et al. 2000; Orsi et al. 2004; Spence et al. 2005). The complete set of maps can be obtained on request to the corresponding author.

The probability contours in Figs. 11, 12 and 13 show areas that will experience mass loadings in excess of 400, 300 and 200 kg/m<sup>2</sup> during the high-, medium- and low-magnitude scenarios, considering the two different vent locations. In the following we discuss the obtained results for the high-, medium- and low-magnitude scenarios separately.

*High-magnitude scenario* For the high-magnitude scenario, the effect of the two variable vent locations on the impact of tephra fallout is almost negligible (Fig. 11). The probability of a mass load in excess of 400 kg/m<sup>2</sup> is greater than 10% (Figs. 11a, a1) in the Campi Flegrei and in the entire city of Naples. However the Campi Flegrei are the sector of the caldera with the highest probability of being invaded by PDC (Orsi et al. 2004). The area with more than 5% probability extends up to the Vesuvian area and its shape is mainly related to wind direction, which disperses the tephra towards the east. For the 300 and 200 kg/m<sup>2</sup> thresholds, the area with more than 5% probability is much wider, extending towards the east up to the Apennines (Figs. 11b, b1, c, c1). The city of Naples has at least 10% probability of being affected by a tephra loading >300 kg/m<sup>2</sup>.

*Medium-magnitude scenario* For this scenario, the two variable vent locations do not generate significant variations in tephra loading effects (Fig. 12). All the iso-load curves have a more circular shape (Fig. 12) compared to those of the high-magnitude scenario, and include the Campi Flegrei and the city of Naples. For a tephra loading >300 kg/m<sup>2</sup>, the entire city of Naples is comprised in the curves with probability value higher than 5% if the eruption vent is located in the Agnano-San Vito area (Fig. 12 b1). Instead, if the vent is located in the Averno-Monte Nuovo area, all the Campi Flegrei, as well the island of Procida, are comprised in the 5% probability curve. However, for both vent locations, the 5% probability contours (Fig. 12b, b1) enclose sectors of the city of Naples and Campi Flegrei

which are outside the area of higher probability of PDC invasion.

*Low-magnitude scenario* For low-magnitude scenario, a different location of the eruption vent produces considerable effects on the probability curves (Fig. 13). All the iso-load curves have a nearly circular shape (Fig. 13) reflecting the distribution of the winds blowing below 10 km (Fig. 10). For a tephra loading >300 kg/m<sup>2</sup>, the probability contours >5% involve the westernmost districts of the city of Naples and the eastern sector of the Campi Flegrei if the eruption vent is located in the Agnano-San Vito area (Fig. 13b1). In the case of a vent location in the Averno-Monte Nuovo area, only the Campi Flegrei are comprised in >5% probability curve (Fig. 13b).

## Conclusions

The obtained results have allowed us to make a step forward in the fallout hazard assessment at the CFC in case of renewal of volcanism in short-mid terms. In fact, tephra-loading hazard maps for the expected high-, medium-, and low-magnitude scenarios, considering a statistical dataset of wind profiles and also two variable vent-area locations, have been constructed. For all the three investigated scenarios, the tephra loading has a significant impact on the densely inhabited Neapolitan–Phlegraean area. The effects of vent location for the high- and medium-magnitude scenarios are not very significant. Whereas the effects on the territory of tephra loading related to the low-magnitude scenario is strongly dependent on the eruption vent location. For the high-magnitude scenario, the area having a probability >5% of a mass load of 300 kg/m<sup>2</sup> extends up to the Vesuvian area. Probability contour 5% of a mass load >300 kg/m<sup>2</sup> enclose sectors of the city of Naples and Campi Flegrei even in the case of a medium-magnitude scenario. For the low-magnitude scenario, the probability curve 5% to have a tephra loading >300 kg/m<sup>2</sup> involve the westernmost districts of the city of Naples only if the eruption vent is located in the Agnano-San Vito area, otherwise Campi Flegrei only are involved. The obtained results may be used for further studies aimed to risk mitigation plans of the Phlegraean-Neapolitan area.

**Acknowledgements** P. Belviso, A. Carandente and M. Tesaro are warmly thanked for the help given in the laboratory work. The research was supported by the Italian Department for Civil Protection within the 2000–2003 and 2004–2006 INGV-DPC Projects. We are also grateful to R. Cioni, C. Hickson and an anonymous referee for their constructive reviews.

## References

- Aitken AC (1935) On least squares and linear combinations of observations. *Proc R Soc Edinb* 55:42–48
- Armenti P, Macedonio G, Pareschi MT (1988) A numerical model for simulation of tephra transport and deposition: Application to May 18, 1980, Mount St. Helens Eruption. *J Geophys Res* 93:6463–6476
- Barberi F, Macedonio G, Pareschi M, Santacroce R (1990) Mapping the tephra fallout risk: an example from Vesuvius (Italy). *Nature* 344:142–144
- Blong RJ (1984) Volcanic hazards: a sourcebook of the effects of eruptions. Academic, Sydney, p 424
- Bursik M (2001) Effect of wind on the rise height of volcanic plumes. *Geophys Res Lett* 18:3621–3624
- Carey S, Sparks RSJ (1986) Quantitative models of the fallout and dispersal of tephra from volcanic eruption columns. *Bull Volcanol* 48:127–141
- Casadevall TJ (ed) (1994) Volcanic ash and aviation safety: proceedings of the First International Symposium on Volcanic Ash and Aviation Safety. US Geol Surv Bull 2047
- Cioni R, Longo A, Macedonio G, Santacroce R, Sbrana A, Sulpizio R, Andronico D (2003) Assessing pyroclastic fall hazard through field data and numerical simulations: example from Vesuvius. *J Geophys Res* 108(B2):2063 DOI 10.1029/2001JB000642
- Civetta L, Orsi G, Pappalardo L, Fisher RV, Heiken G, Ort M (1997) Geochemical zoning, mingling, eruptive dynamics and depositional processes—the campanian ignimbrite, Campi Flegrei caldera, Italy. *J Volcanol Geotherm Res* 75:183–219
- Deino AL, Orsi G, Piochi M, de Vita S (2004) The age of the Neapolitan Yellow Tuff caldera-forming eruption (Campi Flegrei caldera—Italy) assessed by  $^{40}\text{Ar}/^{39}\text{Ar}$  dating method. *J Volcanol Geotherm Res* 133:157–170
- Dellino P, Isaia R, La Volpe L, Orsi G (2001) Statistical analysis of textural data from complex pyroclastic sequence: implication for fragmentation processes of the Agnano-Monte Spina eruption (4.1 ka), Phlegraean Fields, southern Italy. *Bull Volcanol* 63:443–461
- Dellino P, Isaia R, La Volpe L, Orsi G (2004) Interference of particles fallout on the emplacement of pyroclastic surge deposits of the Agnano-Monte Spina eruption (Phlegraean Fields, Southern Italy). *J Volcanol Geotherm Res* 133:193–210
- De Vita S, Orsi G, Civetta L, Carandente A, D'Antonio M, Deino A, di Cesare T, Fisher RV, Isaia R, Marotta E, Necco A, Ort MH, Pappalardo L, Piochi M, Southon J (1999) The Agnano-Monte Spina eruption (4100 years B.P.) in the restless Campi Flegrei caldera. *J Volcanol Geotherm Res* 91:269–301
- De Vivo B, Rolandi G, Gans PB, Calvert A, Bohrsen WA, Spera FJ, Belkin HE (2001) New constraints on the pyroclastic eruptive history of the Campanian volcanic Plain (Italy). *Mineral Petrol* 73:47–65
- Di Girolamo P, Ghiara MR, Lirer L, Munno R, Rolandi G, Stanzione D (1984) Vulcanologia e petrologia dei Campi Flegrei. *Boll Soc Geol It* 103:349–413
- Di Vito MA, Isaia R, Orsi G, Southon J, de Vita S, D'Antonio M, Pappalardo L, Piochi M (1999) Volcanism and deformation in the past 12 ka at the Campi Flegrei caldera (Italy). *J Volcanol Geotherm Res* 91:221–246
- Di Vito MA, D'Antonio M, Braia G, Arienzo I, Civetta L, Di Renzo V, Isaia R, Orsi G, Piermattei M (2004) The Averno 2 eruption in the Campi Flegrei caldera. IAVCEI General Assembly, Pucon, 14–19 November 2004
- Fedele FG, Giaccio B, Isaia R, Orsi G (2003) The Campanian Ignimbrite eruption, Heinrich Event 4, and Palaeolithic change in Europe: a high-resolution investigation. In: Robock A, Oppenheimer C (eds) *Volcanism and the Earth's atmosphere*. Am Geophys Un, Gephys Monog Series. vol. 139. American Geophysical Union, Washington, DC, pp 301–325
- Fisher RV, Orsi G, Ort M, Heiken G (1993) Mobility of large-volume pyroclastic flow—emplacement of the Campanian Ignimbrite, Italy. *J Volcanol Geotherm Res* 56:205–220
- Isaia R, D'Antonio M, Dell'Erba F, Di Vito MA, Orsi G (2004) The Astroni volcano: the only example of close eruptions within the same vent area in the recent history of the Campi Flegrei caldera (Italy). *J Volcanol Geotherm Res* 133:171–192
- Kalnay E, Kanamitsu M, Kister R, Collins W, Deaven D, Gandin L, Iredell M, Saha SGW, Woollen J, Zhu Y, Chelliah M, Ebisuzaki M, Higgins W, Janowiak J, Mo K, Ropelewski C, Wang, J, Leetmaa A, Reynolds R, Jenne R, Joseph D (1996) The NCEP/NCAR 40-years reanalysis project. *Bull Am Meteorol Soc* 77:437–470 (<http://www.cdc.noaa.gov/cdc/reanalysis/>)
- Lirer L, Mastrolorenzo G, Rolandi G (1987) Un evento pliniano nell'attività recente dei Campi Flegrei. *Boll Soc Geol It* 106:461–473
- Lirer L, Petrosino P, Alberico I, Postiglione I (2001) Long-term volcanic hazard forecasts based on Somma-Vesuvio past eruptive activity. *Bull Volcanol* 63:45–60
- Macedonio G, Pareschi MT, Santacroce R (1988) A numerical simulation of the Plinian Fall phase of 79 A.D. eruption of Vesuvius. *J Geophys Res* 93:817–827
- Macedonio G, Pareschi MT, Santacroce R (1990) Renewal of explosive activity at Vesuvius: models for the expected tephra fallout. *J Volcanol Geotherm Res* 40:327–342
- Macedonio G, Costa A, Longo A (2005) A computer model for volcanic ash fallout and assessment of subsequent hazard. *Comput Geosci* 31:837–845
- Miller TP, Casadevall TJ (2000) Volcanic ash hazards to aviation. In: Sigurdsson H, Houghton BF, McNutt SR, Rymer H, Stix J (eds) *Encyclopedia of volcanoes*. Academic, San Diego, pp 915–930
- Mills MJ (2000) Volcanic aerosol and global atmospheric effects. In: Sigurdsson H, Houghton BF, McNutt SR, Rymer H, Stix J (eds) *Encyclopedia of volcanoes*. Academic, San Diego, pp 931–943
- Orsi G, D'Antonio M, de Vita S, Gallo G (1992) The Neapolitan Yellow Tuff, a large-magnitude trachytic phreatoplinitic eruption: eruptive dynamics, magma withdrawal and caldera collapse. *J Volcanol Geotherm Res* 53:275–287
- Orsi G, Civetta L, D'Antonio M, Di Girolamo P, Piochi M (1995) Step-filling and development of a three-layers magma chamber: the Neapolitan Yellow Tuff case history. *J Volcanol Geotherm Res* 67:291–312
- Orsi G, Di Vito M, de Vita S (1996) The restless, resurgent Campi Flegrei Nested Caldera (Italy): constraints on its evolution and configuration. *J Volcanol Geotherm Res* 74:179–214
- Orsi G, Civetta L, Del Gaudio C, de Vita S, Di Vito MA, Isaia R, Petrazzuoli SM, Ricciardi G, Ricco C (1999) Short-term ground deformations and seismicity in the nested Campi Flegrei caldera (Italy): an example of active block-resurgence in a densely populated area. *J Volcanol Geotherm Res* 91:415–451
- Orsi G, de Vita S, Di Vito M, Nave R, Heiken G (2003) Facing volcanic and related hazards in the Neapolitan area. In: Heiken G, Fakundiny R, Sutter J (eds) *Earth sciences in the cities: a reader*. Am Geophys Un, Sp Publ Series. vol. 56. American Geophysical Union, Washington, DC, pp 121–170
- Orsi G, Di Vito MA, Isaia R (2004) Volcanic hazard assessment at the restless Campi Flegrei caldera. *Bull Volcanol* 66:514–530
- Orsi G, di Vito M, Dell'Erba F, Quaglini M, Marzocchi W, Sandri L, Selva J (2007) Assessing volcanic hazards at the restless Campi Flegrei, Italy. *Cities on Volcanoes* 5, Shimabara, 19–23 November 2007
- Ort M, Orsi G, Pappalardo L, Fisher RV (2003) Emplacement processes in a far-traveled dilute pyroclastic current: anisotropy of magnetic susceptibility studies of the Campanian Ignimbrite. *Bull Volcanol* 65:55–72

- Pareschi MT, Cavarra L, Favalli M, Giannini F, Meriggi A (2000) Gis and volcanic risk management. *Nat Hazards* 21:361–379
- Pfeiffer T, Costa A (2004a) A numerical reconstruction of fall deposits from Agnano-Monte Spina (4100 BP) Plinian eruption in the Campi Flegrei area, Italy, Osservatorio Vesuviano-INGV, Naples, Italy, Report (1), Prot. N. 4440 (10.9.2004). <http://www.earth-prints.org/handle/2122/2068>
- Pfeiffer T, Costa A (2004b) Reconstruction and analysis of a sub-Plinian fall deposits from the Astroni volcano (ca. 4100–3800 BP) in the Campi Flegrei area, Italy, Osservatorio Vesuviano-INGV, Naples, Italy, Report (2), Prot. N. 4440 (10.9.2004). <http://www.earth-prints.org/handle/2122/2069>
- Pfeiffer T, Costa A, Macedonio G (2005) A model for the numerical simulation of tephra fall deposits. *J Volcanol Geotherm Res* 140:273–294
- Pyle DM (1989) The thickness, volume and grainsize of tephra fall deposits. *Bull Volcanol* 51:1–15
- Rampino MR, Self S (2000) Volcanism and biotic extinctions. In: Sigurdsson H, Houghton BF, McNutt SR, Rymer H, Stix J (eds) *Encyclopedia of volcanoes*. Academic, San Diego, pp 1083–1091
- Rosi M, Santacroce R (1984) Volcanic hazard assessment in the Phlegraean Fields: a contribution based on stratigraphic and historical data. *Bull Volcanol* 47:359–370
- Rosi M, Sbrana A (1987) The Phlegraean Fields. CNR, Quad de “La ricerca Scientifica” 114:1–175
- Rosi M, Sbrana A, Principe C (1983) The Phlegraean Fields: Structural evolution, volcanic history and eruptive mechanism. *J Volcanol Geotherm Res* 17:273–288
- Rosi M, Vezzoli L, Aleotti P, De Renzi M (1996) Interaction between caldera collapse and eruptive dynamics during the Campanian Ignimbrite eruption, Phlegraean Fields, Italy. *Bull Volcanol* 57:541–554
- Selva J, Marzocchi W, Orsi G, di Vito M, Sandri L, Quaglino M, Costa A (2007) The Bayesian event tree for short- and long-term eruption forecasting (BET\_EF) at Campi Flegrei, Italy. *Cities on Volcanoes 5*, Shimabara, 19–23 November 2007
- Sparks RSJ (1986) The dimensions and dynamics of volcanic eruption columns. *Bull Volcanol* 48:3–15
- Spence R, Kelman I, Baxter PJ, Zuccaro G, Petrazzuoli S (2005) Residential building and occupant vulnerability to tephra fall. *Nat Haz Earth Syst Sci* 5:477–494
- Tilling RI (1989) Volcanic hazards and their mitigation: progress and problems. *Rev Geophys* 27:237–269
- Wohletz K, Orsi G, de Vita S (1995) Eruptive mechanisms of the Neapolitan Yellow Tuff interpreted from stratigraphic, chemical and granulometric data. *J Volcanol Geotherm Res* 67:263–290